

WO₃ AS ADDITIVE FOR EFFICIENT PHOTOCATALYST BINARY SYSTEM TiO₂/WO₃

A. Knoks*, J. Kleperis, G. Bajars, L. Grinberga, O. Bogdanova

Institute of Solid State Physics, University of Latvia,
 8 Kengaraga Str., Riga, LV-1063, LATVIA
 *e-pasts: knoks@cfi.lu.lv

Two different methods of synthesis of TiO₂/WO₃ heterostructures were carried out with the aim to increase photocatalytic activity. In this study, anodic TiO₂ nanotube films were synthesized by electrochemical anodization of titanium foil. WO₃ particles were applied to anodic Ti/TiO₂ samples in two different ways – by electrophoretic deposition (EPD) and insertion during the anodization process. Structural and photocatalytic properties were compared between pristine TiO₂ and TiO₂ with incorporated WO₃ particles. Raman mapping was used to characterise the uniformity of EPD WO₃ coating and to determine the structural composition. The study showed that deposition of WO₃ onto TiO₂ nanotube layer lowered the band gap of the binary system compared to pristine TiO₂ and WO₃ influence on photo-electrochemical properties of titania. The addition of WO₃ increased charge carrier dynamics but did not increase the measured photocurrent response. As the WO₃ undergoes a phase transition from monoclinic to orthorhombic at approximately 320 °C proper sequence WO₃ deposition could be beneficial. It was observed that secondary heat treatment of WO₃ lowers the photocurrent.

Keywords: Anodization, electrophoretic deposition, TiO₂ nanotubes, thin films, TiO₂/WO₃, WO₃.

1. INTRODUCTION

In search of new sustainable energy sources, photocatalysis is a prominent area of research. However, synthesis of materials for an efficient photocatalytic cell still is a great challenge. Titanium dioxide (TiO₂, titania) is extensively studied as a possible

candidate owing to abundance, stability, and synthesis options. Nanostructured titania can be synthesized in a great variety of methods, i.e., sol-gel [1], physical vapour deposition PVD [2], magnetron sputtering [3], electrochemical anodization [4]. The

increased active surface area is desirable; therefore, electrochemical anodization is preferred as anodic TiO₂ forms a self-organized nanotube layer with a high surface area and geometry, enables high charge transfer and electron percolation [5]–[7], and the method is energy and cost-effective with a potential for scale-up [8].

Photocatalytic activity of TiO₂ was discovered only in 1972 by Fujishima and Honda [9], although TiO₂ had been used for decades in various everyday applications, such as gas sensing, colouring pigment, additive for food, toothpaste [10]–[12]. The process of photocatalytic water splitting happens thanks to absorbed photons with energy at least as a band gap of TiO₂, creating electron-hole pair (e-h), which must be separated before recombination [13]. Electrons are collected by current conductor and transferred to the cathode, but holes migrate to the surface and drive a catalytic reaction (splitting H₂O, organic/inorganic pollutants, gas-phase pollutants, etc.) reducing or oxidating molecules [14].

The potential of generated charge carriers must be sufficient to reduce target molecule, TiO₂ conduction and valence bands are at a sufficient level. However, titania has a wide band gap reaching in the UV region ($\lambda \leq 380$ nm), thus limiting the use of sunlight as the light source for activation. Combination of TiO₂ with other photocatalytic materials, which are sensitive in the visible light region, could solve this problem, as it was shown in [15]–[18]. The tungsten trioxide (WO₃) – a comparatively less studied photocatalytically active semiconducting oxide (n-type) – is capable of being acti-

vated by visible light in the blue region with $\lambda \leq 450$ nm [19].

It has been shown that WO₃ incorporation in TiO₂ is a viable method. A single-step anodization process for WO₃-doped TiO₂ nanotubes in an aqueous electrolyte containing the tungsten precursor Na₂WO₄·2H₂O and fluoride ions is characterised by homogenous doping of WO₃ into the TiO₂ nanotube structures [20]. The doping concentration depends on the concentration of the tungsten precursor in the electrolyte, demonstrating that the reported anodizing process is the most efficient approach for metal oxide doping in TiO₂ [21]. For example, the incorporation of WO₃ species onto TiO₂ nanotubes also improved the mercury removal performance due to improved charge separation and decreased charge carrier recombination due to the charge transfer from the conduction band of TiO₂ to the conduction band of WO₃ [22].

In our study, the combination of anodically grown TiO₂ nanotubes with WO₃ is achieved through electrophoretic deposition (EPD) and simultaneous synthesis of TiO₂/WO₃. Anodization of TiO₂ and EPD of WO₃ are time and cost-effective methods, providing high photochemical stability and usage of non-toxic materials. The potential of WO₃ deposition and secondary treatment must be understood for successful TiO₂/WO₃ system description [15], [23]. Single-step Ti anodization with simultaneous incorporating of WO₃ microcrystalline powder was tested by pouring WO₃ into an electrolyte and mixing with a magnetic stirrer during the anodization process.

2. EXPERIMENTAL

TiO₂ nanotubes were synthesized by electrochemically anodizing titanium (Ti)

foil (0.5 mm, Sigma Aldrich) in water-based electrolyte. Ti foil was cleaned and polished

(abrasive material Cr_2O_3 (Sigma Aldrich), average particle size 400 nm), then ultrasonicated for 10 min in acetone (99 % Sigma-Aldrich) and dried in ambient atmosphere. Anodization was performed in two steps: 1) 5 V applied for 10 minutes, 2) 20 V applied for 90 minutes with electrode separation of 2 cm. It is known that anodizing in water based electrolytes requires F^- ions for TiO_2 dissolution as reported by Regonini [24] and Grimes [5]; NaF (Sigma Aldrich) was used as F^- ion source. pH was adjusted with 1M NaOH (Sigma Aldrich) solution until pH level of 4. Anodized samples were rinsed in deionized water and dried in ambient atmosphere. To obtain crystalline TiO_2 samples were heat treated in a furnace at 500 °C for 120 minutes, heating speed 5 °C/min and natural cooling. WO_3 (powder from Sigma Aldrich) was deposited on Ti/TiO_2 via EPD from isopropanol/ HCl electrolyte (both from Sigma Aldrich) in volume ratio 150:1 with WO_3 particles mixed by vigorous stirring and ultrasonication until homogeneous distribution was achieved. EPD process and experimental setup was used similar to the one described by Liepina et al. [15]. Working and auxiliary electrodes were respectively Ti/TiO_2 and platinum foil (0.2 mm, Sigma Aldrich). Deposition was performed for various time intervals under constant

potential. In this study, three sample series were produced indicated with the following identifiers: AT – pristine anodized TiO_2 , EW – deposited WO_3 on anodized TiO_2 and AW – anodized TiO_2 with WO_3 particles present in the electrolyte. Production of AW follows AT procedure, where electrolyte contains dispersed WO_3 particles.

Morphological properties were determined by scanning electron microscope (Phenom Pro). Structural properties were determined by Raman spectroscopy (RENISHAW inVia Raman Microscope) and X-Ray diffraction (X-ray Diffractometer X'Pert Pro MPD, Cu anode, $\lambda = 0.154$ nm). Optical band gap was calculated from reflectance spectra, acquired in 240 to 780 nm range, using integrating sphere in spectrophotometer (Shimadzu SolidSpec-3700). Photoactivity was determined using three-electrode cell, where AT, EW and AW samples were used as working electrode; Pt and calomel (SCE) were used respectively as auxiliary and reference electrodes in 1M NaOH electrolyte. Photoactivity measurement data were collected by potentiostat VoltaLab 40 (PGZ301 Radiometer analytical) while using the visible region of 150 W xenon lamp as a light source. The sample EW synthesis process is shown in Fig. 1.

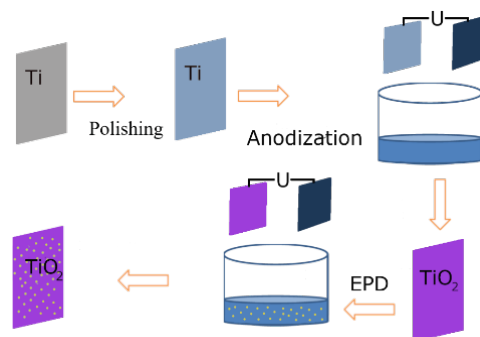


Fig. 1. Sample synthesis procedure: Ti is polished, then anodized in electrolyte without or with WO_3 (in case of single-step AW sample the tungsten oxide particles were dispersed in anodization electrolyte). In a two-step process (below), anodic TiO_2 is heat treated, then WO_3 deposited using EPD.

3. RESULTS AND DISCUSSION

Morphology of the obtained samples was investigated before and after EPD. As it can be seen in SEM images (Fig. 2a),

TiO₂ was synthesized in nanosized tubular forms. EPD of WO₃ covers TiO₂ partially as seen in Fig. 2b.

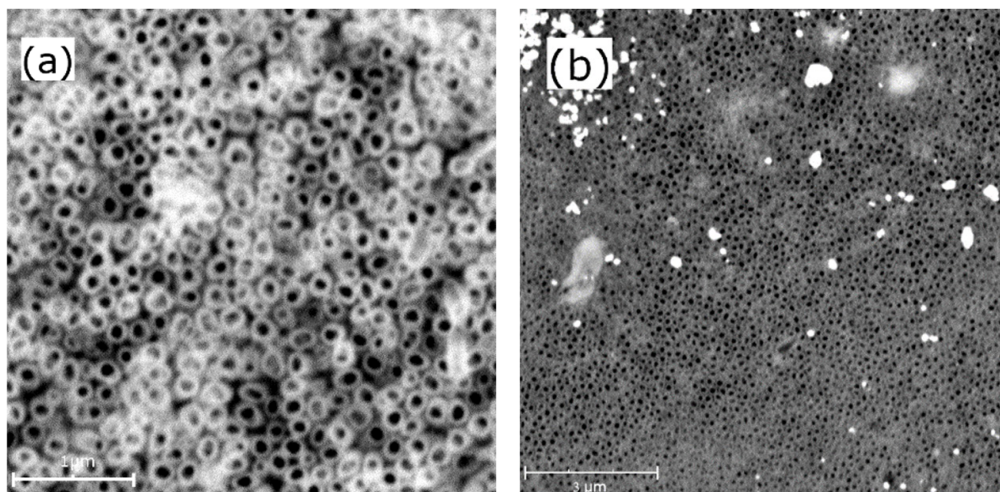


Fig. 2. Morphology investigation with SEM: (a) tubular structures of TiO₂ in an anodized sample, (b) TiO₂ nanotube layer decorated with WO₃ microparticles.

As measured from SEM photo (Fig. 2b), the average dimensions of WO₃ particles are 150–250 nm. It is also seen that microparticles result from the agglomeration of WO₃ nanocrystals, thus indicating the importance of sonication for even distribution as well as appropriate EPD parameters. It is known that amount threshold of WO₃ deposition exists [25], where overdeposition shows lower photo-activity; thus, the only appropriate correct amount can enhance photoelectrochemical properties [15], [26].

Sample crystallinity and the presence of WO₃ and TiO₂ were determined through XRD. As it can be seen in Fig. 3, the WO₃ is present in sample EW, but the AW sample does not show monoclinic WO₃ structure

indicating the undergoing phase transition during sample preparation. The change is clearly seen in the typical 2θ mode intensity of peaks at 22°, 23°, and 24°. The size of WO₃ crystallites was evaluated from Scherrer equation (Patterson et al. [27]), using parameters of the peak $2\theta=23^\circ - 40\pm 5$ nm, whereas TiO₂ crystallite size – 17 ± 3 nm was calculated for $2\theta=25^\circ$. It is well known that crystallite size from XRD scattering is a qualitative indicator. The high-intensity Ti peak in the diffraction spectra comes from the Ti substrate as the radiation penetration is much deeper compared to the overall thickness of the samples. On the other hand, AT samples showed standard TiO₂ anatase phase, i.e., (101) peak at $2\theta = 25^\circ$ was present.

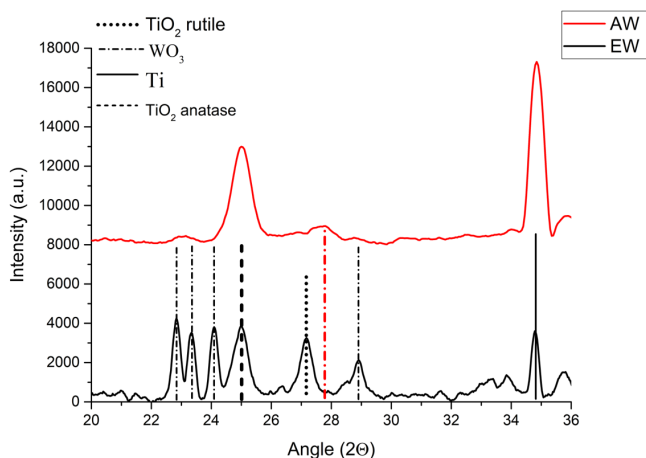


Fig. 3. XRD diffractogram of EW (in black) and AW (in red), strong Ti peaks from the substrate, distinctive WO_3 peaks below 25° , TiO_2 rutile peak at 27° . XRD diffractogram confirms that EW sample contains WO_3 as seen by specific monoclinic peak trio and not present in AW with the absence of those.

Raman investigation shows characteristic WO_3 band at 272 cm^{-1} band (Fig. 4a and 4c), similar to 270 cm^{-1} [28] and 262 cm^{-1} [29]. Particle size directly affects Raman band position, nanosized particles show a shift in Raman band positions [29]. It confirms that our WO_3 has smaller particles, large grain surfaces, and developed grain boundaries, higher concentration of structural defects.

For more comprehensive surface structural composition, the Raman mapping was performed. As seen in Fig. 4 b, c, and d, where phase distribution provides insight not only into the overall phase composition of samples, but also into uniformity of the sample structure. Sample before EPD can be seen in Fig. 4b, it shows TiO_2 composition of two phases, rutile majority with anatase spots. After EPD, WO_3 particles were found on TiO_2 surface as shown in Fig. 4c. It is possible to imagine the particle distribution on the surface using colour differentiation by phase. By assigning a colour to a single-phase the surface phase map can be created as seen in Fig. 4d, where red and green represent TiO_2 and WO_3 , respectively. It shows a single particle on the TiO_2 surface.

Optical band gap (E_{gap}) was determined

from reflectance spectra using Kubelka-Munk equation to find absorption edge by plotting, as seen in Fig. 5, where n is determined by the electron transition nature – indirect allowed transition in case of TiO_2 . The same methodology can be applied for WO_3 – the monoclinic phase has direct allowed transitions and orthorhombic – indirect allowed transitions [30]. Introduction of WO_3 clearly lowers the optical band gap as seen in sample EW (Fig. 5a). Pristine anatase TiO_2 optical band gap is close to the theoretical value of 3.1 eV ; similarly, the AW has 3.1 eV optical band gap. After EPD of WO_3 , the optical band gap lowered to 2.86 eV .

As the directly incorporated WO_3 undergoes heat treatment, anodized titania is amorphous after synthesis, the influence of annealing should be estimated. Samples from EW series were compared as-prepared and with secondary heat treatment. Figure 5b shows that a small increase in the optical band gap is present. Thus, photoelectrochemical properties could also be changed. Diaz-Reyes et al. [31] also reported an increase in the band gap of WO_3 after the heat treatment, where they suggested higher crystallinity and oxygen vacancies as the reason for change.

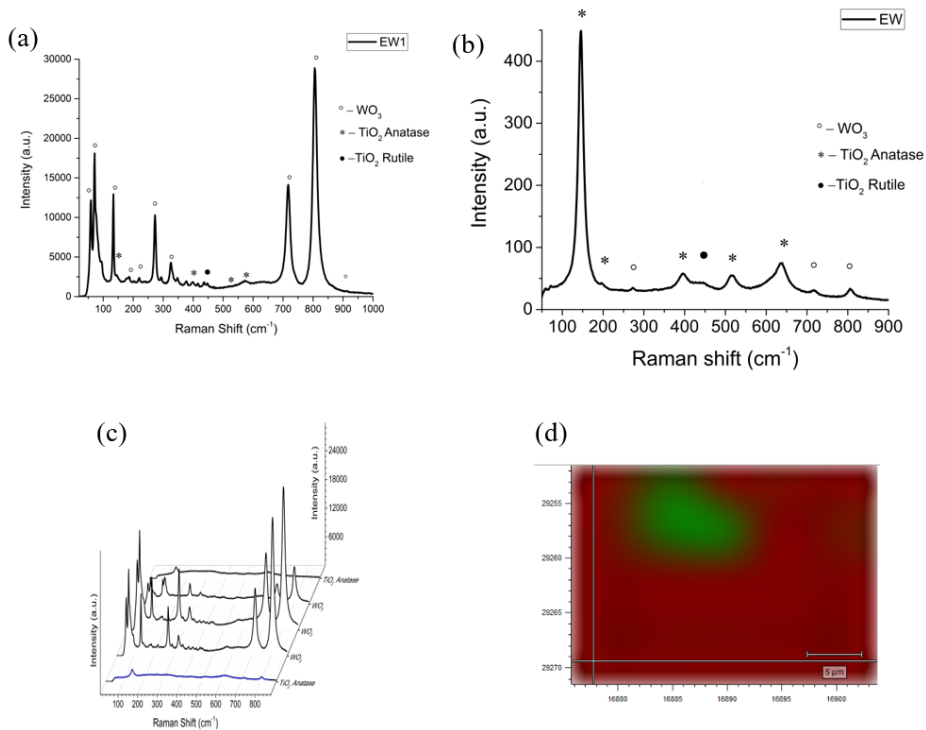


Fig. 4. (a) Raman spectra of WO_3 for EW sample; (b) TiO_2 Raman spectra for EW in another position – clear TiO_2 anatase bands and Rutile bands are seen; (c) Raman mapping of EW sample, WO_3 bands with high intensity and low intensity anatase TiO_2 ; (d) EW sample in 2D composition/structural distribution of both materials – TiO_2 (red), WO_3 (green).

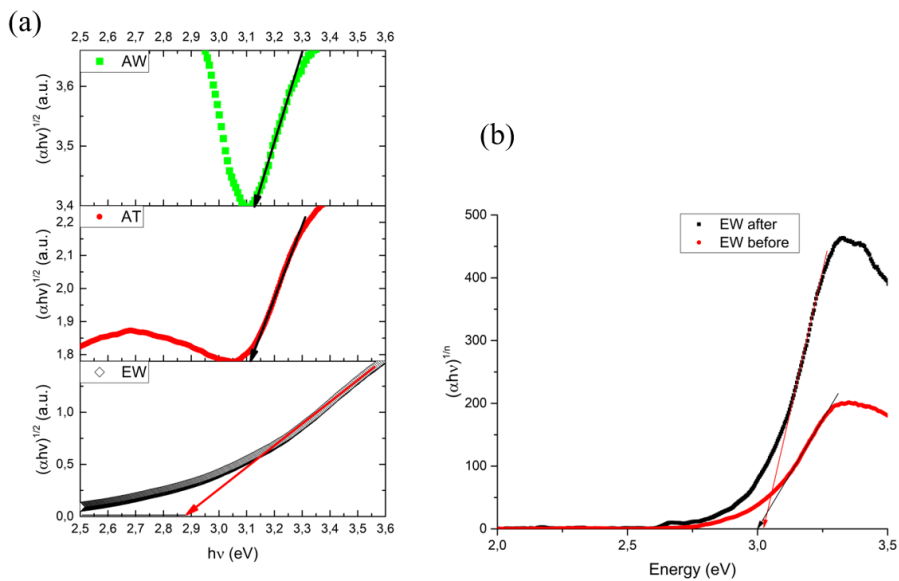


Fig. 5. (a) E_{gap} comparison between various samples; (b) optical band gap comparison for WO_3/TiO_2 deposited with EPD before and after heat treatment.

Photoactivity was determined by measuring photocurrent response (PCR) – voltage transient characteristics – see Fig. 6c, and open circuit potential (OCP) – see Fig. 6b and 6d. In addition, the Mott-Schottky method was used to determine charge carrier density. Comparing PCR values for samples before and after EPD there can be an increase in PCR and OCP values as provided in the literature showing that WO₃ deposition on TiO₂ can have a positive effect on photoactivity.

Upon deposition of WO₃ a certain limit has to be maintained, as overdeposition of WO₃ has a negative impact on photoactivity as seen in Fig. 6a. A test sample in EW series was overdeposited and ultrasonically cleaned to decrease WO₃ amount on the surface; OCP value rose again as seen in Fig. 6a red plot. In this study, for EPD the electric field was kept at 5–6 V/cm considering lower necessary deposition time. With higher deposition times, the film thickness easily saturates within minutes with deposited layer over 60 μm, lowering a photo-electrochemical activity as shown in Fig. 6a. Such observation supports the necessity to find equilibrium and even distribution of WO₃ particles on TiO₂ for an increase in activity. Similar findings were reported by Khoo et al. [25]. Comparing annealing influence on the PCR and OCP, PCR and OCP decreased by 70 % and 75 %, respectively (see Fig. 6b). The change could be attributed to change in crystallinity and phase transition from

monoclinic to triclinic as seen in structural analysis. Thus, it is not surprising that sample AW provides similar results, showing 55 % and 36 % decrease in OCP and PCR, respectively, and EW shows 65 % and 48 % decrease, respectively, as seen in Fig. 6c and d as well as in Table 1. Though, it is noteworthy that AW shows higher charge carrier dynamics indicating more rapid higher charge carrier separation compared to AT dynamics, where reaching plato takes more time. Dynamics can be seen in Fig. 6c – PCR and Fig. 6d – OCP.

Amount of WO₃ on/in TiO₂ is critical for a higher photocatalytic activity, which is confirmed by existence of WO₃ amount threshold for the increased photo-physical activity [10]. Existence of a threshold is determined by generated charge carrier interfacial transfer, thereof it stops over the threshold when most of the light is absorbed by WO₃ and as material with lower photocurrent values the result shows overall lower photocurrent. It can be assumed that generated e-h pairs go through charge interfacial transfer, hole from valence band (V_B) of WO₃ to V_B of TiO₂ and e⁻ from TiO₂ conduction band (C_B) to WO₃ C_B. Estimation of charge carrier density shows that addition of WO₃ in both series (EW and AW) provides with two orders of magnitude higher charge carrier density compared to AT samples. For AW, the great change is seen in PCR dynamics, but an absolute value did not increase.

Table 1. Summary of Results (OCP and PCR – photoactivity, E_{gap} – optical band, E_{Fb} – flat band potential and N_D – charge carrier density)

| Sample | OCP, mV | PCR, μA/cm ² | E _{gap} , eV | E _{Fb} , mV | N _D (cm ⁻³) |
|--------|------------|-------------------------|-----------------------|----------------------|------------------------------------|
| AT | -222.6±4.7 | 4.01±0.79 | 3.11±0.04 | -1919.4±0.2 | 4.7·10 ¹⁷ |
| EW | -80.5 | 2.07 | 2.86 | -668.8 | 1.6·10 ²¹ |
| AW | -99.3 | 2.63 | 3.13 | -799.3 | 6.1·10 ²¹ |

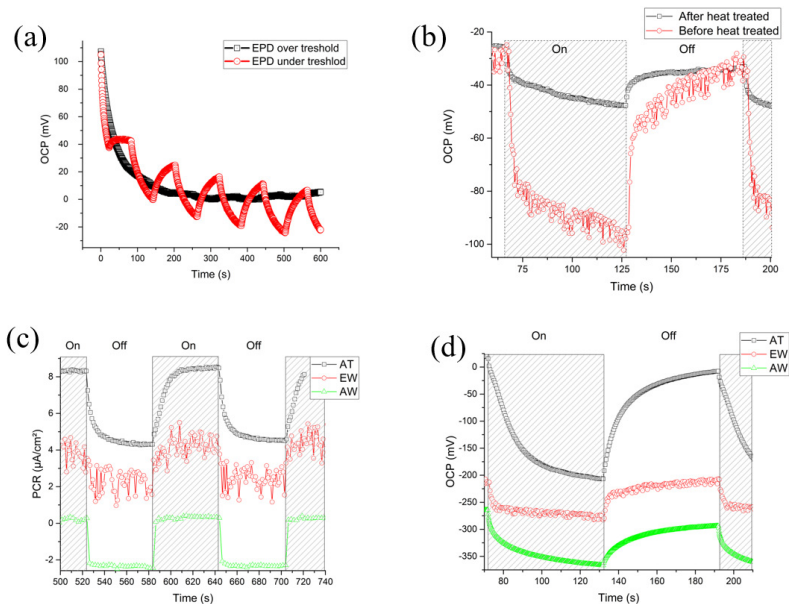


Fig. 6. Sample photoactivity dependence and comparison. (a) OCP value comparison of WO₃ deposition amount. Overdeposition decreases OCP. (b) OCP value comparison for WO₃ before and after heat treatment. (c) PCR comparison of samples, AW has the highest charge separation, EW shows low PCR values and a high recombination rate. (d) OCP comparison for samples, AT shows the highest OCP.

4. CONCLUSIONS

In this study, different methods of synthesis and investigation of Ti/TiO₂/WO₃ system were carried out. Firstly, anodic titania was synthesized. Secondly, electrophoretic deposition of WO₃ particles on the surface of an anodically grown TiO₂ nanotube layer done. Thirdly, a single-step Ti anodization with simultaneous incorporating of WO₃ microcrystalline powder was performed by the addition of WO₃ in the anodization process. Morphological and structural investigation of samples showed that WO₃ formed separated “islands” on TiO₂ nanotube film in EPD and incorporated WO₃ in TiO₂ nanotubes in the single-step method. Characteristic WO₃ band shifts in Raman spectroscopy were observed after annealing, indicating the change in crystallinity of WO₃, the same was seen in XRD diffrac-

tograms. The presence of Raman bands, as well as XRD provided clear evidence of synthesis of Ti/TiO₂/WO₃ system. In the study, the addition of WO₃ introduced lower OCP, PCR values even though the optical band gap was lowered, and charge carrier density increased.

As anodic titania required annealing after synthesis, monoclinic WO₃ particle introduction did not show promise for increased photoactivity in the visible range due to a decrease in photoactivity after heating. Similarly, overdeposition of WO₃ in the EPD method on TiO₂ lowered the photo-response of samples. However, it does not exclude the possibility of a specific ratio and/or introduction of WO₃/TiO₂ for an increase in photo-response. The introduction of tungsten atoms directly into

TiO₂ structures could be beneficial through organic tungsten acids or substituting anodization cathode. Lowered activity is explained with additional trapping sites on the WO₃ grain boundaries, as well as lower WO₃ photo-activity compared to pristine

TiO₂, despite the increase in charge carrier density. Further research on the incorporation of W into TiO₂ will be carried out to investigate charge carrier transfer and the increased photoactivity.

ACKNOWLEDGEMENTS

The financial support provided by Scientific Research Project for Students and Young Researchers No. SJZ/2018/9 implemented at the Institute of Solid State Physics, University of Latvia is greatly acknowledged. Institute of Solid State Physics,

University of Latvia as the Center of Excellence has received funding from the European Union's Horizon 2020 Framework Programme H2020-WIDESPREAD-01-2016-2017-TeamingPhase2 under grant agreement No. 739508, project CAMART².

REFERENCES

1. Ahn, Y. (2003). Variation of Structural and Optical Properties of Sol-Gel TiO₂ Thin Films with Catalyst Concentration and Calcination Temperature. *Materials Letters*, 57 (30), 4660–4666.
2. Hasan, M. M., Haseeb, A. S. M. A., Saidur, R., & Masjuki, H. H. (2008). Effects of Annealing Treatment on Optical Properties of Anatase TiO₂ Thin Films. *International Journal of Mechanical, Aerospace, Industrial, Mechatronic and Manufacturing Engineering*, 2, 410–414.
3. Daviðsdóttir, S., Shabadi, R., Galca, A. C., Andersen, I. H., Dirscherl, K., & Ambat, R. (2014). Investigation of DC Magnetron-Sputtered TiO₂ Coatings: Effect of Coating Thickness, Structure, and Morphology on Photocatalytic Activity. *Applied Surface Science*, 313, 677–686.
4. Regonini, D., & Clemens, F. J. (2015). Anodized TiO₂ Nanotubes: Effect of Anodizing Time on Film Length, Morphology and Photoelectrochemical Properties. *Materials Letters*, 142, 97–101.
5. Grimes, C. A., & Mor, G. K. (2009). *TiO₂ Nanotube Arrays*. Boston, MA: Springer US.
6. Sofiane, S., & Bilel, M. (2016). Effect of Specific Surface Area on Photoelectrochemical Properties of TiO₂ Nanotubes, Nanosheets and Nanowires Coated with TiC Thin Films. *Journal of Photochemistry and Photobiology A: Chemistry*, 324, 126–133.
7. Arifin, K., Yunus, R. M., Minggu, L. J., & Kassim, M. B. (2021). Improvement of TiO₂ nanotubes for Photoelectrochemical Water Splitting: Review. *International Journal of Hydrogen Energy*, 46 (7), 4998–5024.
8. Khaw, J. S., Curioni, M., Skeldon, P., Bowen, C. R., & Cartmell, S. H. (2019). A Novel Methodology for Economical Scale-Up of TiO₂ Nanotubes Fabricated on Ti and Ti Alloys. *Journal of Nanotechnology*, 2019.
9. Fujishima, A., & Honda, K. (1972). Electrochemical Photolysis of Water at a Semiconductor Electrode. *Nature*, 238 (5358), 37–38.
10. Varghese, O. K., Gong, D., Paulose, M., Ong, K. G., & Grimes, C. A. (2003). Hydrogen Sensing Using Titania Nanotubes. *Sensors and Actuators B: Chemical*, 93 (1–3), 338–344.

11. Wu, H., & Zhang, Z. (2011). High Photoelectrochemical Water Splitting Performance on Nitrogen Doped Double-Wall TiO₂ Nanotube Array Electrodes. *International Journal of Hydrogen Energy*, 36 (21), 13481–13487.
12. Ismail, A. A., & Bahnemann, D. W. (2014). Photochemical Splitting of Water for Hydrogen Production by Photocatalysis: A Review. *Solar Energy Materials and Solar Cells*, 128, 85–101.
13. Osterloh, F. E. (2008m) Inorganic Materials as Catalysts for Photochemical Splitting of Water. *Chemistry of Materials*, 20 (1), 35–54.
14. Qamar, M., Drmosh, Q., Ahmed, M. I., Qamaruddin, M., & Yamani, Z. H. (2015). Enhanced Photoelectrochemical and Photocatalytic Activity of WO₃-Surface Modified TiO₂ Thin Film. *Nanoscale Research Letters*, 10 (1), 54.
15. Liepina, I., Bajars, G., Rublans, M., Kleperis, J., Lasis, A., & Pentjuss, E. (2015). Structure and Photocatalytic Properties of TiO₂-WO₃ Composites Prepared by Electrophoretic Deposition. *IOP Conference Series: Materials Science and Engineering*, 77 (1), 012039.
16. Rong, X., Qiu, F., Zhang, C., Fu, L., Wang, Y., & Yang, D. (2015). Preparation, Characterization and Photocatalytic Application of TiO₂-Graphene Photocatalyst under Visible Light Irradiation. *Ceramics International*, 41 (2), 2502–2511.
17. Lu, X., Ma, Y., Tian, B., & Zhang, J. (2011). Preparation and Characterization of Fe–TiO₂ Films with High Visible Photoactivity by Autoclaved-Sol Method at Low Temperature. *Solid State Sciences*, 13 (3), 625–629.
18. Ola, O., & Maroto-Valer, M. M. (2015). Transition Metal Oxide Based TiO₂ Nanoparticles for Visible Light Induced CO₂ Photoreduction. *Applied Catalysis A: General*, 502, 114–121.
19. Amano, F., Ishinaga, E., & Yamakata, A. (2013). Effect of Particle Size on the Photocatalytic Activity of WO₃ Particles for Water Oxidation. *Journal of Physical Chemistry C*, 117 (44), 22584–22590.
20. Riboni, F., Bettini, L. G., Bahnemann, D. W., & Selli, E. (2013). WO₃-TiO₂ vs. TiO₂ Photocatalysts: Effect of the W Precursor and Amount on the Photocatalytic Activity of Mixed Oxides. *Catalysis Today*, 209, 28–34.
21. Yoo, H., Oh, K., Nah, Y. C., Choi, J., & Lee, K. (2018). Single-Step Anodization for the Formation of WO₃-Doped TiO₂ Nanotubes toward Enhanced Electrochromic Performance. *ChemElectroChem*, 5 (22), 3379–3382.
22. Lee, W. H., Lai, C. W., & Abd Hamid, S. B. (2015). In Situ Anodization of WO₃-Decorated TiO₂ Nanotube Arrays for Efficient Mercury Removal. *Materials*, 8 (9), 5702–5714.
23. Nazari, M., Golestani-Fard, F., Bayati, R., & Eftekhari-Yekta, B. (2015). Enhanced Photocatalytic Activity in Anodized WO₃-Loaded TiO₂ Nanotubes. *Superlattices and Microstructures*, 80 (4), 91–101.
24. Regonini, D., Bowen, C. R. R., Jaroenworarluck, A., & Stevens, R. (2013). A Review of Growth Mechanism, Structure and Crystallinity of Anodized TiO₂ Nanotubes. *Materials Science and Engineering R: Reports*, 74 (12), 377–406.
25. Khoo, E., Lee, P. S., & Ma, J. (2010). Electrophoretic Deposition (EPD) of WO₃ Nanorods for Electrochromic Application. *Journal of the European Ceramic Society*, 30 (5), 1139–1144.
26. Lai, C. W., & Sreekantan, S. (2013). Incorporation of WO₃ Species into TiO₂ Nanotubes via Wet Impregnation and their Water-Splitting Performance. *Electrochimica Acta*, 87, 294–302.
27. Patterson, A. L. (1939), The Scherrer Formula for X-Ray Particle Size Determination. *Physical Review*, 56 (10), 978–982.
28. Hunge, Y. M., Mahadik, M. A., Moholkar, A. V., & Bhosale, C. H. (2017). Photoelectrocatalytic Degradation of Oxalic Acid Using WO₃ and Stratified WO₃/TiO₂ Photocatalysts under Sunlight Illumination. *Ultrasonics Sonochemistry*, 35, 233–242.
29. Cai, Z.-X., Li, H.-Y., Ding, J.-C., & Guo, X. (2017). Hierarchical Flowerlike WO₃ Nanostructures Assembled by Porous Nanoflakes for Enhanced NO Gas Sensing. *Sensors and Actuators B: Chemical*, 246, 225–234.

30. Kleperis, J., Zubkans, J., & Lusis, A. R. (1997). Nature of fundamental absorption edge of WO₃. In E. A. Silinsh, A. Medvids, A. R. Lusis, & A. O. Ozols (Eds.), *Optical Organic and Semiconductor Inorganic Materials* (vol. 2968, pp. 186–191). International Society for Optics and Photonics.
31. Diaz-Reyes, J., Flores-Mena, J. E., Gutierrez-Arias, J. M., Morin-Castillo, M. M., Azucena-Coyotecatl, H., Galván, M., ... & Mendez-López, A. (2010). Optical and structural properties of WO₃ as a function of the annealing temperature. In *Proceedings of the 3rd WSEAS international Conference on Advances in Sensors, Signals and Materials* (pp. 99–104), 3–5 November 2010, Faro, Portugal. World Scientific and Engineering Academy and Society (WSEAS).